

Broadband near total light absorption in non- PT -symmetric waveguide-cavity systems

YIN HUANG,^{1,2,*} CHANGJUN MIN,² AND GEORGIOS VERONIS^{3,4}

¹Department of Optoelectrics Information Science and Engineering, School of Physics and Electronics, Central South University, Changsha, Hunan 410012, China

²Key Laboratory of Optoelectronic Devices and Systems of Ministry of Education and Guangdong Province, Shenzhen University, Shenzhen 518060, China

³School of Electrical Engineering and Computer Science, Louisiana State University, Baton Rouge, LA 70803, USA

⁴Center for Computation and Technology, Louisiana State University, Baton Rouge, LA 70803, USA

*yhuan15@csu.edu.cn

Abstract: We introduce broadband waveguide absorbers with near unity absorption. More specifically, we propose a compact non-parity-time-symmetric perfect absorber unit cell, consisting of two metal-dielectric-metal (MDM) stub resonators with unbalanced gain and loss side-coupled to a MDM waveguide, based on unidirectional reflectionlessness at exceptional points. With proper design, light can transport through the perfect absorber unit cell with reflection close to zero in a broad wavelength range. By cascading multiple unit cell structures, the overall absorption spectra are essentially the superposition of the absorption spectra of the individual perfect absorber unit cells, and absorption of $\sim 100\%$ is supported in a wide range of frequencies.

© 2016 Optical Society of America

OCIS codes: (240.6680) Surface plasmons; (130.2790) Guided waves; (230.7370) Waveguides; (230.4555) Coupled resonators.

References and links

1. N. I. Landy, S. Sajuyigbe, J. J. Mock, D. R. Smith, and W. J. Padilla, "Perfect metamaterial absorber," *Phys. Rev. Lett.* **100**, 207402 (2008).
2. S. Longhi, " PT -symmetric laser absorber," *Phys. Rev. A* **82**, 031801 (2010).
3. J. R. Piper and S. Fan, "Total absorption in a graphene monolayer in the optical regime by critical coupling with a photonic crystal guided resonance," *ACS Photon.* **1**, 347–353 (2014).
4. R. Feng, W. Ding, L. Liu, L. Chen, J. Qiu, and G. Chen, "Dual-band infrared perfect absorber based on asymmetric T-shaped plasmonic array," *Opt. Express* **22**, A335–A343 (2014).
5. Y. Cui, K. Fung, J. Xu, H. Ma, Y. Jin, S. He, and N. X. Fang, "Ultrabroadband light absorption by a sawtooth anisotropic metamaterial slab," *Nano Lett.* **12**, 1443–1447 (2012).
6. S. Yu, X. Piao, J. Hong, and N. Park, "Progress toward high-Q perfect absorption: a Fano antilaser," *Phys. Rev. A* **92**, 011802 (2015).
7. L. Huang and H. Chen, "A brief review on terahertz metamaterial perfect absorbers," *Terahertz Sci. Technol.* **6**, 26–39 (2013).
8. K. Aydin, V. E. Ferry, R. M. Briggs, and H. A. Atwater, "Broadband polarization-independent resonant light absorption using ultrathin plasmonic super absorbers," *Nat. Commun.* **2**, 517 (2011).
9. J. Sun, L. Liu, G. Dong, and J. Zhou, "An extremely broad band metamaterial absorber based on destructive interference," *Opt. Express* **19**, 21155–21162 (2011).
10. L. Huang, D. R. Chowdhury, S. Ramani, M. T. Reiten, S. Luo, A. J. Taylor, and H. Chen, "Experimental demonstration of terahertz metamaterial absorbers with a broad and flat high absorption band," *Opt. Lett.* **37**, 154–156 (2012).
11. C. Yang, C. Ji, W. Shen, K. Lee, Y. Zhang, X. Liu, and L. J. Guo, "Compact multilayer film structures for ultrabroadband, omnidirectional, and efficient absorption," *ACS Photon.* **3**, 590–596 (2016).
12. D. Gagnon, S. Kocabas, and D. A. B. Miller, "Characteristic impedance model for plasmonic metal slot waveguides," *IEEE J. Sel. Top. Quantum Electron.* **14**, 1473–1478 (2008).
13. C. Min and G. Veronis, "Absorption switches in metal-dielectric-metal plasmonic waveguides," *Opt. Express* **17**, 10757–10766 (2009).
14. Y. Gong, X. Liu, H. Lu, L. Wang, and G. Wang, "Perfect absorber supported by optical Tamm states in plasmonic waveguide," *Opt. Express* **19**, 18393–18398 (2011).

15. Z. Lin, H. Ramezani, T. Eichelkraut, T. Kottos, H. Cao, and D. N. Christodoulides, "Unidirectional invisibility induced by PT -symmetric periodic structures," *Phys. Rev. Lett.* **106**, 213901 (2011).
16. A. Regensburger, C. Bersch, M. A. Miri, G. Onishchukov, D. N. Christodoulides, and U. Peschel, "Parity-time synthetic photonic lattices," *Nature* **488**, 167–171 (2012).
17. L. Ge, Y. D. Chong, and A. D. Stone, "Conservation relations and anisotropic transmission resonances in one-dimensional PT -symmetric photonic heterostructures," *Phys. Rev. A* **85**, 023802 (2012).
18. L. Feng, Y. L. Xu, W. S. Fegadolli, M. H. Lu, J. E. B. Oliveira, V. R. Almeida, Y. F. Chen, and A. Scherer, "Experimental demonstration of a unidirectional reflectionless parity-time metamaterial at optical frequencies," *Nat. Mater.* **12**, 108–113 (2013).
19. A. Mostafazadeh, "Invisibility and PT symmetry," *Phys. Rev. A* **87**, 012103 (2013).
20. C. Hahn, S. Song, C. Oh, and P. Berini, "Single-mode lasers and parity-time symmetry broken gratings based on active dielectric-loaded long-range surface plasmon polariton waveguides," *Opt. Express* **23**, 19922–19931 (2015).
21. Y. Fu, Y. Xu, and H. Chen, "Zero index metamaterials with PT symmetry in a waveguide system," *Opt. Express* **24**, 1648–1657 (2016).
22. A. Manjavacas, "Anisotropic optical response of nanostructures with balanced gain and loss," *ACS Photon.* **3**, 1301–1307 (2016).
23. X. Yin and X. Zhang, "Unidirectional light propagation at exceptional points," *Nat. Mater.* **12**, 175–177 (2013).
24. L. Feng, X. Zhu, S. Yang, H. Zhu, P. Zhang, X. Yin, Y. Wang, and X. Zhang, "Demonstration of a large-scale optical exceptional point structure," *Opt. Express* **22**, 1760–1767 (2014).
25. Y. Shen, X. H. Deng, and L. Chen, "Unidirectional invisibility in a two-layer non- PT -symmetric slab," *Opt. Express* **22**, 19440–19447 (2014).
26. M. Kang, H. Cui, T. Li, J. Chen, W. Zhu, and M. Premaratne, "Unidirectional phase singularity in ultrathin metamaterials at exceptional points," *Phys. Rev. A* **89**, 065801 (2014).
27. Y. Huang, G. Veronis, and C. Min, "Unidirectional reflectionless propagation in plasmonic waveguide-cavity systems at exceptional points," *Opt. Express* **23**, 29882–29895 (2015).
28. E. Yang, Y. Lu, Y. Wang, Y. Dai, and P. Wang, "Unidirectional reflectionless phenomenon in periodic ternary layered material," *Opt. Express* **24**, 14311–14321 (2016).
29. S. A. R. Horsley, M. Artoni, and G. C. La Rocca, "Spatial Kramer-Kronig relations and the reflection of waves," *Nat. Photonics* **9**, 436–439 (2015).
30. W. L. Barnes, A. Dereux, and T. W. Ebbesen, "Surface plasmon subwavelength optics," *Nature (London)* **424**, 824–830 (2003).
31. F. Nazari, N. Bender, H. Ramezani, M. K. Moravvej-Farshi, D. N. Christodoulides, and T. Kottos, "Optical isolation via PT -symmetric nonlinear Fano resonances," *Opt. Express* **22**, 9574–9584 (2014).
32. L. Chang, X. Jiang, S. Hua, C. Yang, J. Wen, L. Jiang, G. Li, G. Wang and M. Xiao, "Parity-time symmetry and variable optical isolation in active-passive-coupled microresonators," *Nat. Photonics* **8**, 524–529 (2014).
33. K. Wang, Z. Yu, S. Sandhu, and S. Fan, "Fundamental bounds on decay rates in asymmetric single-mode optical resonators," *Opt. Lett.* **38**, 100–102 (2013).
34. C. Manolatou, M. J. Khan, S. Fan, P. R. Villeneuve, H. A. Haus, and J. D. Joannopoulos, "Coupling of modes analysis of resonant channel add-drop filters," *IEEE J. Sel. Top. Quantum Electron.* **35**, 1322–1331 (1999).
35. Z. Yu, G. Veronis, and S. Fan "Gain-induced switching in metal-dielectric-metal plasmonic waveguides," *Appl. Phys. Lett.* **92**, 041117 (2008).
36. P. Neutens, P. Van Dorpe, I. De Vlamincq, L. Lagae, and G. Borghs, "Electrical detection of confined gap plasmons in metal-insulator-metal waveguides," *Nat. Photonics* **3**, 283–286 (2009).
37. L. Yang, C. Min, and G. Veronis, "Guided subwavelength slow-light mode supported by a plasmonic waveguide system," *Opt. Lett.* **35**, 4184–4186 (2010).
38. Y. Huang, C. Min, and G. Veronis, "Subwavelength slow-light waveguides based on a plasmonic analogue of electromagnetically induced transparency," *Appl. Phys. Lett.* **99**, 143117 (2011).
39. G. Cao, H. Li, Y. Deng, S. Zhan, Z. He, and B. Li, "Plasmon-induced transparency in a single multimode stub resonator," *Opt. Express* **22**, 25215–25223 (2014).
40. Y. Huang, C. Min, P. Dastmalchi, and G. Veronis, "Slow-light enhanced subwavelength plasmonic waveguide refractive index sensors," *Opt. Express* **23**, 14922–14936 (2015).
41. E. N. Economou, "Surface plasmons in thin films," *Phys. Rev.* **182**, 539–554 (1969).
42. Y. Salamin, W. Heni, C. Haffner, Y. Fedoryshyn, C. Hoessbacher, R. Bonjour, M. Zahner, D. Hillerkuss, P. Leuchtmann, D. L. Elder, L. R. Dalton, C. Hafner, and J. Leuthold, "Direct conversion of free space millimeter waves to optical domain by plasmonic modulator antenna," *Nano Lett.* **15**, 8342–8346 (2015).
43. G. Veronis, R. W. Dutton, and S. Fan, "Method for sensitivity analysis of photonic crystal devices," *Opt. Lett.* **29**, 2288–2290 (2004).
44. E. D. Palik, *Handbook of Optical Constants of Solids* (Academic, 1985).
45. J. Jin, *The Finite Element Method in Electromagnetics* (Wiley, 2002).
46. D. Pacifici, H. J. Lezec, L. A. Sweatlock, C. D. Ruiter, V. Ferry, and H. A. Atwater, "All-optical plasmonic modulators and interconnects," in *Plasmonic nanoguides and circuits*, S. I. Bozhevolnyi, ed. (World Scientific, 2009).
47. M. P. Nezhad, K. Tetz, and Y. Fainman, "Gain assisted propagation of surface plasmon polaritons on planar metallic

- waveguides,” *Opt. Express* **12**, 4072–4079 (2004).
48. H. Ramezani, H. Li, Y. Wang, and X. Zhang, “Unidirectional spectral singularities,” *Phys. Rev. Lett.* **113**, 263905 (2014).
 49. Q. Gan, Z. Fu, Y. Ding, and F. J. Bartoli, “Ultrawide-bandwidth slow-light system based on THz plasmonic graded metallic grating structures,” *Phys. Rev. Lett.* **112**, 256803 (2008).
 50. T. Pickering, J. M. Hamm, A. F. Page, S. Wuestner, and O. Hess, “Cavity-free plasmonic nanolasing enabled by dispersionless stopped light,” *Nat. Commun.* **52**, 4972 (2014).
 51. V. E. Babicheva, I. V. Kulkova, R. Malureanu, K. Yvind, and A. V. Lavrinenko, “Plasmonic modulator based on gain-assisted metal-semiconductor-metal waveguide,” *Photon. Nanostructures* **10**, 389–399 (2012).
 52. H. Carrere, V. G. Truong, X. Marie, R. Brenot, G. De Valicourt, F. Lelarge, and T. Amand, “Large optical bandwidth and polarization insensitive semiconductor optical amplifiers using strained InGaAsP quantum wells,” *Appl. Phys. Lett.* **97**, 121101 (2010).
 53. X. Zhang, Y. Li, T. Li, S. Lee, C. Feng, L. Wang, and T. Meis, “Gain-assisted propagation of surface plasmon polaritons via electrically pumped quantum wells,” *Opt. Lett.* **35**, 3075–3077 (2010).
 54. N. Kirstaedter, O. G. Schmidt, N. N. Ledentsov, D. Bimberg, V. M. Ustinov, A. Yu. Egorov, A. E. Zhukov, M. V. Maximov, P. S. Kopev, and Zh. I. Alferov, “Gain and differential gain of single layer InAs/GaAs quantum dot injection lasers,” *Appl. Phys. Lett.* **69**, 1226 (1996).
 55. A. Mahigir, P. Dastmalchi, W. Shin, S. Fan, and G. Veronis, “Plasmonic coaxial waveguide-cavity devices,” *Opt. Express* **23**, 20549–20562 (2015).
 56. F. N. Xia, L. Sekaric, and Y. Vlasov, “Ultracompact optical buffers on a silicon chip,” *Nat. Photonics* **1**, 65–71 (2007).
 57. M. Notomi, E. Kuramochi, and T. Tanabe, “Large-scale arrays of ultrahigh-Q coupled nanocavities,” *Nat. Photonics* **2**, 741–747 (2008).

1. Introduction

Near-perfect absorbers show great promise for photovoltaics, thermal emission, invisibility and interferometric applications [1–6]. Several previously proposed perfect absorbers have narrow bandwidth and reflect a fairly large amount of the total incident energy [1–4]. Absorbers based on the slow light effect [5], metamaterials [7–10], and multilayer film structures with graded refractive index profile [11] have been proposed in order to broaden the absorption band. Waveguide-based perfect absorbers can lead to applications in all-optical photonic devices, such as photodetectors and switches [12, 13]. Waveguide-based perfect absorbers may also be highly desired in multichannel filters to prevent crosstalk between adjacent channels [11]. Recently, Gong *et al.* proposed a narrowband perfect absorber using the optical Tamm states in a plasmonic metal-dielectric-metal (MDM) waveguide [14].

Broadband near-perfect absorption can be realized when broadband reflectionless light propagation is achieved in the absorber structures. In the past few years, it has been proposed using parity-time (*PT*) symmetric optical structures to attain broadband unidirectional light reflectionlessness at exceptional points by careful modulation of the refractive index profile [15–22]. However, because gain and loss compensate each other, the transmission in the classical gain/loss balanced *PT*-symmetric grating structures is unity when light is reflectionless from one side at the exceptional points based on the generalized conservation relation [15, 17], and thus, the absorption in general is zero [22]. Unidirectional light reflectionlessness can also be attained in non-*PT*-symmetric structures with unbalanced gain and loss (or even without gain) [23–29]. This is due to the fact that exceptional points exist in a larger family of non-Hermitian Hamiltonians [23]. Nevertheless, most of these non-*PT*-symmetric structures attain unidirectional reflectionlessness only at a specific frequency [24–27]. Although Yang *et al.* demonstrated broadband unidirectional reflectionless light transport at the exceptional point in a periodic ternary layered structure consisting of lossy and lossless dielectrics [28], large-size periodic structures are not easy to implement in dense integrated optical chips. Most recently, Horsley *et al.* showed theoretically that broadband unidirectional invisibility can be realized in planar inhomogeneous dielectric media, in which the spatial distributions of the real and imaginary parts of the dielectric permittivity are related by Kramers-Kronig relations [29]. In practice, realizing such a complicated permittivity profile is challenging.

In this paper, we introduce a non- PT -symmetric waveguide-cavity system, which consists of two resonators with gain and loss side-coupled to a waveguide. Plasmonic waveguides have shown the potential to guide and manipulate light at deep subwavelength scales [30]. We propose a compact non-periodic perfect absorber unit cell, based on the unidirectional reflectionless propagation at exceptional points. Several previously proposed non- PT -symmetric optical systems support unidirectional reflectionless propagation only at a specific frequency [24-27]. Here we present an analysis of the broadband unidirectional near-zero reflection propagation in the proposed absorber unit cell structure. We find that, with proper design, the perfect absorption condition coincides with the broadband near-zero reflection condition, and show that light can transport through the proposed compact non- PT -symmetric perfect absorber unit cells with near-zero reflection in a broad wavelength range. We also show that, by properly cascading the unit cell structures, broadband near-total absorption can be realized.

The remainder of the paper is organized as follows. In Section 2, we employ temporal coupled mode theory (CMT) to account for the behavior of the proposed waveguide-cavity system. In Subsection 3.1, we use this theory to design a perfect absorber unit cell structure based on a non- PT -symmetric plasmonic waveguide system. The realized broadband near-zero reflection is then investigated in Subsection 3.2. In Subsection 3.3, we design a broadband waveguide absorber with near-unity absorption by cascading the perfect absorber unit cell structures designed in Subsection 3.1. Finally, our conclusions are summarized in Section 4.

2. Theory and design method

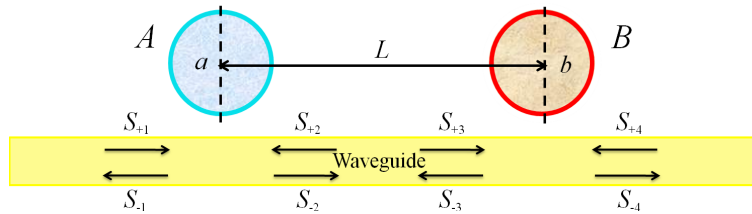


Fig. 1. Schematic of a waveguide side coupled to two resonators. Both resonators have a symmetry plane perpendicular to the waveguide. S_1^+ and S_2^+ are the amplitudes of the incoming waves to resonator A from the forward and backward directions, respectively; S_1^- and S_2^- are the amplitudes of the outgoing waves from resonator A. S_3^+ , S_4^+ and S_3^- , S_4^- are similarly defined for resonator B.

The schematic of a perfect absorber unit cell, which consists of two single mode optical resonators side coupled to waveguide with a single propagating mode, is shown in Fig. 1. Recently, waveguide-cavity structures were used for the realization of on-chip optical diodes in PT -symmetric optical systems [31, 32]. Light transport in the structure of Fig. 1 can be described using CMT [33, 34]. For harmonic time dependence of $e^{-j\omega t}$, the time evolution of the mode amplitudes a and b of resonators A (left) and B (right), respectively, can be described by the following equations:

$$\frac{da}{dt} = (j\omega_{01} - \frac{1}{\tau_{01}} - \frac{1}{\tau_1})a + \kappa_1 S_{+1} + \kappa_2 S_{+2}, \quad (1)$$

$$\frac{db}{dt} = (j\omega_{02} - \frac{1}{\tau_{02}} - \frac{1}{\tau_2})b + \kappa_3 S_{+3} + \kappa_4 S_{+4}, \quad (2)$$

where ω_{01} and ω_{02} are the resonance frequencies of resonators A and B, respectively. In addition, κ_1 , κ_2 are the input coupling coefficients into resonator A associated with the forward and

backward propagating modes in the waveguide, respectively, and κ_3, κ_4 are similarly defined for resonator B . $1/\tau_i, i = 1, 2$, are the decay rates of the resonator mode amplitudes due to the power escape through the waveguide, $1/\tau_{0i}, i = 1, 2$, are the decay (growth) rates due to the internal loss (gain) in the resonators, and L is the distance between the two resonators. S_1^+ and S_2^+ are the amplitudes of the incoming waves to resonator A from the forward and backward directions, respectively, while S_1^- and S_2^- are the amplitudes of the outgoing waves from resonator A . S_3^+, S_4^+ and S_3^-, S_4^- are similarly defined for resonator B . Based on power conservation, the rate of change of the energy in the resonator mode must be equal to the difference between the incoming and outgoing power, and the outgoing waves of the resonators are [33,34]

$$S_{-1} = S_{+2} - \kappa_2^* a, \quad S_{-2} = S_{+1} - \kappa_1^* a, \quad (3)$$

$$S_{-3} = S_{+4} - \kappa_4^* b, \quad S_{-4} = S_{+3} - \kappa_3^* b, \quad (4)$$

where $S_{+3} = S_{-2}e^{-\gamma L}$, $S_{+2} = S_{-3}e^{-\gamma L}$, and $\gamma = \alpha + j\beta$ is the complex propagation constant of the propagating mode in the waveguide. Due to the perpendicular symmetry plane of the resonators, we have $\kappa_1 = \kappa_2$, and $\kappa_3 = \kappa_4$. Note that $\kappa_1 = \sqrt{\frac{1}{\tau_1}}e^{j\theta_1}$, and $\kappa_3 = \sqrt{\frac{1}{\tau_2}}e^{j\theta_2}$, where $\theta_i, i = 1, 2$, are the phases of the coupling coefficients [33,34]. Solving the above coupled-mode equations, the reflection and transmission spectra can be expressed as

$$R_f = |r_f^2| = \left| \frac{\frac{-2}{\tau_1\tau_2} + (j\Delta\omega_2 + \frac{1}{\tau_{c2}})\frac{e^{2\gamma L}}{\tau_1} + (j\Delta\omega_1 + \frac{1}{\tau_{c1}})\frac{1}{\tau_2}}{\frac{-1}{\tau_1\tau_2} + (j\Delta\omega_1 + \frac{1}{\tau_{c1}})(j\Delta\omega_2 + \frac{1}{\tau_{c2}})e^{2\gamma L}} \right|^2, \quad (5)$$

$$R_b = |r_b^2| = \left| \frac{\frac{-2}{\tau_1\tau_2} + (j\Delta\omega_1 + \frac{1}{\tau_{c1}})\frac{e^{2\gamma L}}{\tau_2} + (j\Delta\omega_2 + \frac{1}{\tau_{c2}})\frac{1}{\tau_1}}{\frac{-1}{\tau_1\tau_2} + (j\Delta\omega_1 + \frac{1}{\tau_{c1}})(j\Delta\omega_2 + \frac{1}{\tau_{c2}})e^{2\gamma L}} \right|^2, \quad (6)$$

$$T = |t^2| = \left| \frac{(j\Delta\omega_1 + \frac{1}{\tau_{01}})(j\Delta\omega_2 + \frac{1}{\tau_{02}})}{\frac{-1}{\tau_1\tau_2} + (j\Delta\omega_1 + \frac{1}{\tau_{c1}})(j\Delta\omega_2 + \frac{1}{\tau_{c2}})e^{2\gamma L}} \right|^2, \quad (7)$$

where $\Delta\omega_i = \omega - \omega_{0i}, i = 1, 2$, $\frac{1}{\tau_{ci}} = \frac{1}{\tau_{0i}} + \frac{1}{\tau_i}, i = 1, 2$, t is the complex transmission coefficient, while r_f and r_b are the complex reflection coefficients for light incident from the left (forward direction) and right (backward direction), respectively. Thus, when the system is lossless ($\frac{1}{\tau_{01}} = \frac{1}{\tau_{02}} = 0$ and $\alpha = 0$), the reflection coefficients for light incident in the forward and backward directions are the same ($R_f = R_b$). On the contrary, when the system is lossy, while the transmission coefficients in the forward and backward directions are the same, the reflection coefficients in the forward and backward directions are in general different.

Here we assume that the resonant frequencies ω_{01}, ω_{02} , and decay rates $\frac{1}{\tau_1}, \frac{1}{\tau_2}$ are the same for the two resonators, that is $\omega_{01} = \omega_{02} = \omega_0$, and $\frac{1}{\tau_1} = \frac{1}{\tau_2} = \frac{1}{\tau}$. The reason that we make this assumption will become clear in Subsection 3.2. In order to achieve complete absorption in the structure of Fig. 1, both the transmission and reflection have to be zero. Based on Eq. (7), when light is incident on the structure in the forward direction, the transmission T is zero, if the following condition is satisfied

$$\omega = \omega_0, \quad \frac{1}{\tau_{01}} = 0 \text{ or } \frac{1}{\tau_{02}} = 0. \quad (8)$$

In addition, based on Eq. (5), the on resonance reflection $R_f(\omega = \omega_0)$ is zero, if the following condition is satisfied

$$\left(\frac{1}{\tau_02} + \frac{1}{\tau}\right)e^{2\gamma(\omega_0)L} + \left(\frac{1}{\tau_01} - \frac{1}{\tau}\right) = 0. \quad (9)$$

Here, we choose $\frac{1}{\tau_{02}} = 0$. If the waveguide is lossless ($\gamma = j\beta$), using the above two equations we obtain

$$\cos[2\beta(\omega_0)L] = -1, \frac{1}{\tau_{01}} = \frac{2}{\tau}, \frac{1}{\tau_{02}} = 0. \quad (10)$$

If the waveguide is lossy ($\gamma = \alpha + j\beta$), combining Eqs. (8) and (9) leads to

$$\cos[2\beta(\omega_0)L] = -1, \frac{1}{\tau_{01}} = \frac{e^{2\alpha L} + 1}{\tau}, \frac{1}{\tau_{02}} = 0. \quad (11)$$

In both Eqs. (10) and (11), the decay rate $\frac{1}{\tau_{01}}$ due to internal loss in resonator *A* is positive, which requires that the left resonator (resonator *A*) be filled with an absorptive material. The absorption for light incident from the forward direction for the system of Fig. 1 can be calculated as $A_f = 1 - R_f - T$. Thus, if Eq. (10) [Eq. (11)] is satisfied in the lossless (lossy) waveguide case, we obtain perfect absorption for light incident from the forward direction for the system of Fig. 1. We also note that the condition $\cos(2\beta L) = -1$ is satisfied when the distance between the two resonators L is equal to odd multiples of a quarter of the guide wavelength [$L = (2n + 1)\lambda_g/4$].

3. Results

In this section, we use a non-*PT*-symmetric plasmonic-waveguide cavity system, consisting of two MDM stub resonators side coupled to a MDM waveguide [Fig. 2(a)], to realize perfect absorption based on the theory discussed in the previous section. Among different plasmonic waveguiding structures, MDM plasmonic waveguides, which are the optical analogue of microwave two conductor transmission lines [13], are of particular interest [35-40], because they support modes with deep subwavelength scale over a very wide range of frequencies extending from DC to visible [41], and are relatively easy to fabricate [42].

We use a two-dimensional finite-difference frequency-domain (FDFD) method [43] to numerically calculate the transmission and reflection coefficients in the plasmonic waveguide structure. This method allows us to directly use experimental data for the frequency-dependent dielectric constant of metals such as silver [44], including both the real and imaginary parts, with no approximation. Perfectly matched layer (PML) absorbing boundary conditions are used at all boundaries of the simulation domain [45].

3.1. Perfect absorber unit cell

Figure 2(b) shows the transmission and reflection spectra for the structure of Fig. 2(a) calculated for light incident from both the forward and backward directions using full-wave FDFD simulations (solid lines) and CMT (circles) for $w = 50$ nm, $w_1 = 10$ nm, $w_2 = 25$ nm, $h_1 = 67.5$ nm, and $h_2 = 53$ nm. We observe that there is very good agreement between the CMT results and the exact results. The distance between the two stubs is chosen to be $L = 285$ nm, so that $\cos(2\beta L) = -1$ [Eq. (11)]. The dielectric is air, and the metal is silver. The left and right stubs are filled with silicon dioxide doped with CdSe quantum dots ($\epsilon_A = 4.0804 - j0.6$) [13,46] and InGaAsP ($\epsilon_B = 11.38 + j0.41$) [35,47], respectively. The stub dimensions are chosen so that their resonant frequencies are equal $\omega_{01} = \omega_{02} = \omega_0 = 2\pi 193.4$ THz ($\lambda_0 = 1.55\mu\text{m}$), and their decay rates due to power escape through the waveguide are also equal $\frac{1}{\tau_1} = \frac{1}{\tau_2} = \frac{1}{\tau}$. In the presence of pumping, optical gain and loss can be achieved using InGaAsP and silicon dioxide doped with CdSe quantum dots, respectively [13, 35]. The imaginary part of the dielectric constant of the gain material filling the right stub (0.41) is chosen to compensate the material loss in the metal ($\frac{1}{\tau_{02}} = 0$), so that the right stub behaves essentially as a lossless stub [35]. In addition, the imaginary part of the dielectric constant of the absorptive material filling the left stub (-0.6) is chosen to satisfy the condition $\frac{1}{\tau_{01}} = \frac{e^{2\alpha L} + 1}{\tau}$ [Eq. (11)]. Such gain and loss coefficients are within the limits of currently experimentally achievable values [13, 35, 46, 47].

Figure 2(b) also shows the absorption spectra in the forward direction calculated using FDFD (green solid line). The numerical results of Fig. 2(b) show that the structure of Fig. 2(a), which includes loss and gain, is unidirectional reflectionless at $f = 193.4$ THz ($R_f = 0$, $R_b \neq 0$). More interestingly, the results confirm that the on resonance reflection in the backward direction is unity, as predicted by CMT [Eq. (6)]. Thus, for light incident from the left the on resonance absorption is unity, while for light incident from the right the on resonance reflection is unity [Fig. 2(b)]. As expected by reciprocity, the on resonance transmission for light incident from both the forward and backward directions is zero.

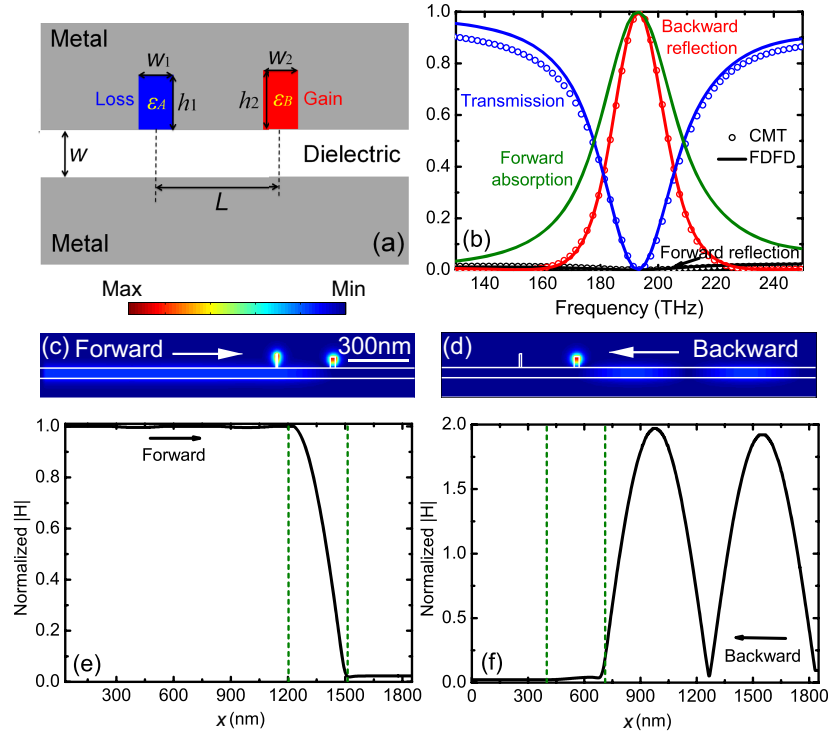


Fig. 2. (a) Schematic of a perfect absorber unit cell consisting of a MDM plasmonic waveguide side coupled to two MDM stub resonators. (b) Reflection and transmission spectra for the structure of Fig. 2(a) calculated for light incident from both the forward and backward directions using FDFD (solid lines) and CMT (circles). Results are shown for $w = 50$ nm, $w_1 = 10$ nm, $w_2 = 25$ nm, $h_1 = 67.5$ nm, and $h_2 = 53$ nm. The left and right stubs are filled with silicon dioxide doped with CdSe quantum dots ($\epsilon_A = 4.0804 - j0.6$) and InGaAsP ($\epsilon_B = 11.38 + j0.41$), respectively. Also shown are the absorption spectra in the forward direction calculated using FDFD (green solid line). (c) and (d) Magnetic field amplitude profiles for the structure of Fig. 2(a) at $f = 193.4$ THz ($\lambda_0 = 1.55 \mu\text{m}$), when the fundamental TM mode of the MDM waveguide is incident from the left and right, respectively. All parameters are as in Fig. 2(b). (e) and (f) Magnetic field amplitude in the middle of the MDM waveguide, normalized with respect to the field amplitude of the incident fundamental TM waveguide mode in the middle of the waveguide, when the mode is incident from the left and right, respectively. The two vertical dashed lines indicate the left boundary of the left stub, and the right boundary of the right stub. All parameters are as in Fig. 2(b).

The total absorption in the forward direction can be observed in the magnetic field distributions. When the waveguide mode is incident from the right (backward direction), there is no

transmission, and the incident and reflected fields form a strong interference pattern [Figs. 2(d) and 2(f)]. On the other hand, when the waveguide mode is incident from the left (forward direction), there is hardly any reflection and transmission [Figs. 2(c) and 2(e)].

In fact, at the resonant frequency ($f_0 = 193.4$ THz), the right stub is lossless ($\frac{1}{\tau_{02}} = 0$), so that it behaves as a perfect reflector. It has a role similar to the one of perfect mirrors or metallic ground planes in classical layered absorbers, such as Salisbury screens, which are based on critical coupling [3, 8–10]. For light incident from the left on resonance, the wave directly reflected from the left stub, and the decaying amplitude into the backward direction of the resonant cavity fields of the left stub resonator, as well as of the resonator formed between the two stubs interfere destructively, so that the reflection R_f reduces to zero, and the system becomes a perfect absorber.

We note here that the optical properties of our proposed two-port system can also be described by the optical scattering matrix of the system which relates the amplitudes of the incoming and the outgoing waves [27]. In the presence of loss, such a system is analogous to open quantum systems which are characterized by complex non-Hermitian Hamiltonians [18, 23, 24, 27], and there is a close analogy between optical scattering matrices and Hamiltonian matrices [15, 16, 18, 24, 27]. When the optical scattering matrix eigenvalues coalesce into a single eigenvalue, and the eigenstates coalesce into a single eigenstate, the system exhibits an exceptional point [27]. This leads to unidirectional reflectionless propagation in either the forward or the backward direction. Thus, in the plasmonic system of Fig. 2(a) the existence of an exceptional point on resonance leads to unidirectional reflectionless propagation [$R_f(\omega = \omega_0) = 0, R_b(\omega = \omega_0) \neq 0$]. In addition, since the on resonance backward reflection is unity [$R_b(\omega = \omega_0) = 1$] [Fig. 2(b)], the on resonance transmission is zero, and the system therefore exhibits unidirectional total absorption [$A_f(\omega = \omega_0) = 1, A_b(\omega = \omega_0) = 0$].

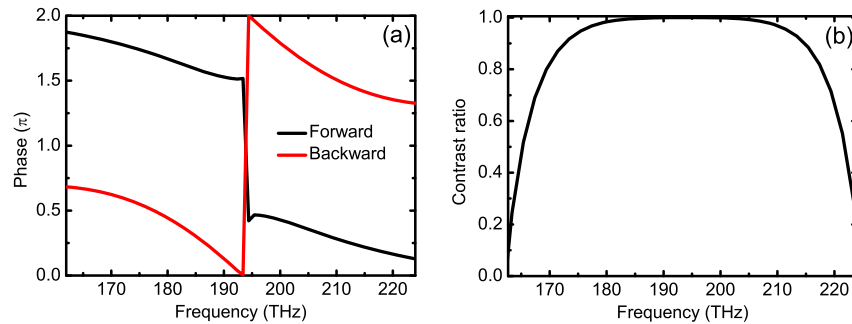


Fig. 3. Phase spectra of the reflection coefficients in the forward (r_f , black) and backward (r_b , red) directions for the structure of Fig. 2(a). All parameters are as in Fig. 2(b). (b) Contrast ratio spectra for the structure of Fig. 2(a). All parameters are as in Fig. 2(b).

In Fig. 3(a), we observe that the phase of the reflection coefficient in the forward direction r_f undergoes an abrupt π jump, when the frequency is crossing over the exceptional point on resonance, which actually resembles the phase transition from the PT -symmetric phase to the PT broken phase in optical PT -symmetric systems [17, 18, 24, 26, 27]. In contrast, the phase of the reflection coefficient r_b in the backward direction in general varies smoothly with frequency [26, 27]. However, Fig. 3(a) shows that the phase of the reflection coefficient in the backward direction r_b undergoes an abrupt jump. This is due to the fact that the right stub acts as a perfect reflector for light coming from the right on resonance ($f = f_0 = 193.4$ THz) [Figs. 2(d) and 2(f)]. When resonance trapping occurs for reflection, the corresponding delay time, which is proportional to the time that the light is trapped in the stub, diverges. Here the delay time is defined as $\tau_r = \frac{d\theta_r}{d\omega}$, where θ_r is the argument of the reflection coefficient [48].

3.2. Broadband unidirectional reflectionlessness of perfect absorber unit cell

Broadband total absorption becomes possible only when broadband reflectionless light propagation can be achieved in the absorber structures. However, non- PT -symmetric optical systems typically exhibit unidirectional reflectionless propagation only within a very narrow wavelength range around the exceptional point [24-27]. This is especially true for non-periodic non- PT -symmetric systems, which are relatively easy to fabricate and more compact. This, however, limits potential applications of compact non- PT -symmetric optical systems as broadband perfect absorbers. In addition, an optical medium that satisfies the PT -symmetry condition can behave as a coherent perfect absorber, fully absorbing incoming coherent waves with appropriate amplitudes and phases injected from both sides of the medium [2]. The underlying mechanism of such a PT -symmetric coherent perfect absorber is not based on the unidirectional reflectionlessness at exceptional points. However, such PT -symmetric coherent perfect absorbers also exhibit total absorption only at specific frequencies, and are not reflectionless in a broad wavelength range [2].

In this subsection, we investigate the broadband unidirectional near-zero reflection in our proposed non- PT -symmetric perfect absorber unit cell structure [Fig. 2(a)], which was introduced in the previous section. We consider the general case without making any assumptions, and derive the general conditions for broadband near-zero reflection in the forward direction. From Eq. (5), zero reflection in the forward direction ($R_f = 0$) leads to

$$\begin{cases} -\frac{1}{\tau_1\tau_2} + \frac{1}{\tau_{01}\tau_2} - \frac{(\omega - \omega_{02})\sin(2\beta L)}{\tau_1} e^{2\alpha L} + \frac{\cos(2\beta L)}{\tau_1} \left(\frac{1}{\tau_{02}} + \frac{1}{\tau_2}\right) e^{2\alpha L} = 0, \\ \left[\frac{\cos(2\beta L)}{\tau_1} e^{2\alpha L} + \frac{1}{\tau_2}\right]\omega - \frac{\omega_{01}}{\tau_2} - \frac{\omega_{02}\cos(2\beta L)}{\tau_1} e^{2\alpha L} + \frac{\sin(2\beta L)}{\tau_1} \left(\frac{1}{\tau_{02}} + \frac{1}{\tau_2}\right) e^{2\alpha L} = 0. \end{cases} \quad (12)$$

Broadband zero reflection in the forward direction ($R_f = 0$) requires the solution of Eq. (12) to be weakly dependent on frequency. To meet this requirement, we set the terms in Eq. (12) which include ω equal to zero and obtain

$$\sin(2\beta L) = 0, \text{ and } \frac{\cos(2\beta L)}{\tau_1} e^{2\alpha L} + \frac{1}{\tau_2} = 0. \quad (13)$$

Since $\frac{1}{\tau_1}$ and $\frac{1}{\tau_2}$, which are the decay rates of the field in the resonators due to the power escape through the waveguide, are both positive, we must have $\cos(2\beta L) = -1$, and we therefore obtain

$$\frac{e^{2\alpha L}}{\tau_1} = \frac{1}{\tau_2}. \quad (14)$$

Substituting $\cos(2\beta L) = -1$ and Eq. (14) into Eq. (12), we obtain

$$\frac{\omega_{02}}{\tau_1} e^{2\alpha L} = \frac{\omega_{01}}{\tau_2}, \text{ and } \frac{1}{\tau_2\tau_{01}} - \frac{1}{\tau_1\tau_2} (e^{2\alpha L} + 1) - \frac{e^{2\alpha L}}{\tau_1\tau_{02}} = 0. \quad (15)$$

When αL is small, $e^{2\alpha L} \sim 1$, and Eqs. (14), (15) become

$$\frac{1}{\tau_2} = \frac{1}{\tau_1} = \frac{1}{\tau}, \omega_{01} = \omega_{02}, \text{ and } \frac{1}{\tau_{01}} = \frac{1}{\tau} (e^{2\alpha L} + 1) + \frac{1}{\tau_{02}}. \quad (16)$$

These are the general conditions for broadband near-zero reflection in the forward direction ($R_f = 0$) for our proposed waveguide-cavity system. Thus, to achieve broadband near-zero reflection, the conditions $\frac{1}{\tau_1} = \frac{1}{\tau_2}$ and $\omega_{01} = \omega_{02}$ have to be satisfied. This is the reason that we chose $\frac{1}{\tau_1} = \frac{1}{\tau_2} = \frac{1}{\tau}$ and $\omega_{01} = \omega_{02} = \omega_0$ in Section 2. We note that for frequencies far away from the resonant frequency ω_0 , the denominator of Eq. (5) is proportional to $(\omega - \omega_0)^4$

(note that $\omega_{01} = \omega_{02} = \omega_0$), whereas the numerator is only proportional to $(\omega - \omega_0)^2$. Thus, the reflection R_f remains small even when the frequency is not in the vicinity of the resonant frequency ω_0 , and the system exhibits broadband near-zero reflection. We also note that for our proposed perfect absorber unit cell structure, the decay rate $\frac{1}{\tau_{02}}$ was chosen zero [Eqs. (10) and (11)], and thus the broadband unidirectional near-zero reflection condition [Eq. (16)] coincides with the perfect absorption condition [Eq. (11)].

In Fig. 2(b) we indeed observe that our proposed non- PT -symmetric perfect absorber structure shown in Fig. 2(a) exhibits near-zero reflection in the forward direction over a broad wavelength range (black). For the range of frequencies shown, the maximum reflection is less than 2%. In addition, the contrast ratio between the forward and backward reflection, defined as $\eta = \left| \frac{R_f - R_b}{R_f + R_b} \right|$ [18], as a function of frequency for the structure of Fig. 2(b) is shown in Fig. 3(b). The contrast ratio between the forward and backward reflection is higher than 99% from 180.4 THz to 207.4 THz. In contrast to the perfect mirrors used in the layer based perfect absorbers [3, 9, 10], the right stub in our proposed structure is not a perfect reflector off-resonance. This enables our structure to have the broadband near-zero reflection property discussed above.

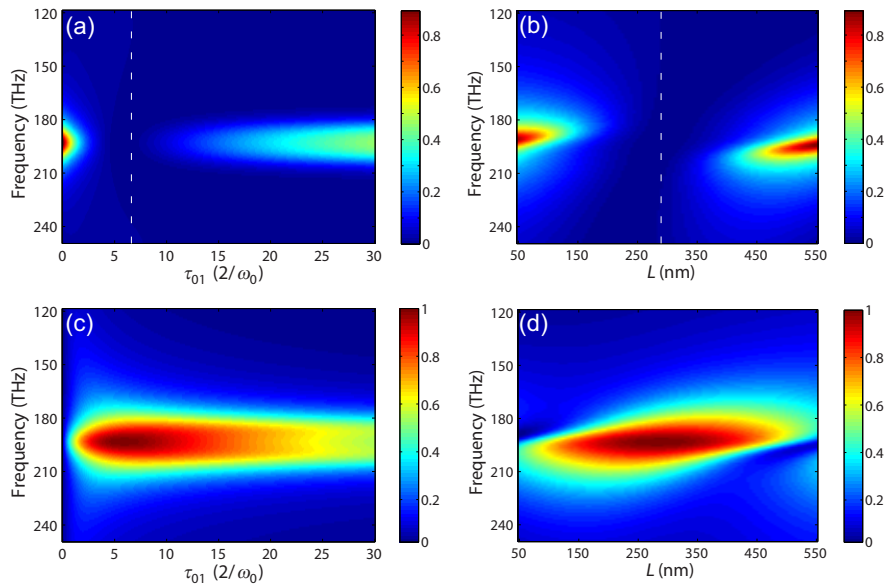


Fig. 4. (a) Reflection spectra in the forward direction (R_f) as a function of the life time τ_{01} for the structure of Fig. 2(a). All other parameters are as in Fig. 2(b). (b) Reflection spectra in the forward direction (R_f) as a function of the distance L for the structure of Fig. 2(a). All other parameters are as in Fig. 2(b). (c) Absorption spectra in the forward direction as a function of the life time τ_{01} for the structure of Fig. 2(a). All other parameters are as in Fig. 2(b). (d) Absorption spectra in the forward direction as a function of the distance L for the structure of Fig. 2(a). All other parameters are as in Fig. 2(b).

Figure 4(a) shows the reflection spectra in the forward direction as a function of the life time τ_{01} for the structure of Fig. 2(a). All other parameters are as in Fig. 2(b). Note that $\frac{1}{\tau_{01}}$ is the decay rate due to internal loss in the left stub resonator (resonator A). This decay rate $\frac{1}{\tau_{01}}$ can be controlled by tuning the absorption coefficient of the material filling the left resonator. At $f = f_0 = 193.4$ THz, when $\frac{1}{\tau_{01}} \rightarrow \frac{2}{\tau}$, or equivalently $\text{Im}(\epsilon_A) \rightarrow -0.6$ [note that this is equivalent to $\tau_{01} \rightarrow 6(2/\omega_0)$, where $\frac{\omega_0}{2\pi} = 193.4$ THz, and corresponds to the white dashed line in Fig. 4(a)], the reflection in the forward direction R_f of the proposed unit cell structure of Fig. 2(a) goes

to zero, and the near-zero reflection band broadens. If $\frac{1}{\tau_{01}}$ further increases, the reflection R_f begins to increase [Fig. 4(a)]. Since the right stub is a perfect reflector at $f = f_0 = 193.4$ THz (transmission of the unit cell structure is zero), total absorption is also achieved when $R_f = 0$ for $\tau_{01} = 6 (2/\omega_0)$ [Fig. 4(c)]. In other words, in order to obtain broadband unidirectional near-zero reflection [$R_f(\omega) \cong 0$], and perfect absorption [$A_f(\omega_0) = 1$] in the forward direction, the loss in the left stub resonator should be appropriately tuned.

Figure 4(b) shows the reflection spectra in the forward direction as a function of the distance between the two resonators L for the structure of Fig. 2(a). All other parameters are as in Fig. 2(b). We observe that approximately zero reflection R_f can be obtained for different L . However, broadband near-zero reflection can only be realized when $L = 285$ nm [white dashed line in Fig. 4(b)], which is obtained from $\cos(2\beta L) = -1$ at $f = 193.4$ THz, and corresponds to a quarter of the guide wavelength ($L = \lambda_g/4$). Perfect absorption in the forward direction is also obtained for $L = 285$ nm [Fig. 4(d)].

3.3. System with broadband near-total absorption

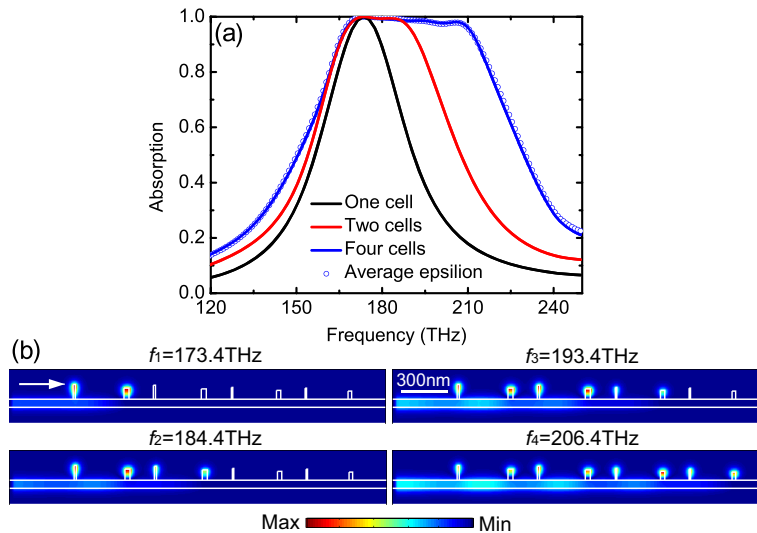


Fig. 5. (a) Absorption spectra for structures with different number of perfect absorber unit cells calculated using FDFD. Results are shown for $w = 50$ nm, and distance between two adjacent unit cells of 150 nm. For the structure with four different unit cells, the parameters for each cell [Fig. 2(a)] are $w_1 = 12.5, 12.5, 10, 10$ nm, $w_2 = 30, 30, 25, 25$ nm, $h_1 = 85, 80, 67.5, 62.5$ nm, $h_2 = 65, 60, 57.5, 47.5$ nm, $L = 320, 300, 285, 267.5$ nm, $\epsilon_A = 4.0804 - j0.78, 4.0804 - j0.76, 4.0804 - j0.6, 4.0804 - j0.58$, and $\epsilon_B = 11.38 + j0.4, 11.38 + j0.38, 11.38 + j0.41, 11.38 + j0.42$. Also shown are the absorption spectra for a four-unit cell system where the same material properties are used in all unit cells ($\epsilon_A = 4.0804 - j0.68, \epsilon_B = 11.38 + j0.4$) (shown with blue circles), which are obtained by averaging the properties (ϵ_A and ϵ_B) of the four unit cells used before. (b) Magnetic field distributions at four different frequencies of 173.4, 184.4, 193.4, and 206.4 THz, when the waveguide mode is incident from the left. All other parameters are as in Fig. 5(a).

Taking advantage of the broadband near-zero reflection property of the proposed non-*PT*-symmetric perfect absorber unit cell of Fig. 2(a), we next cascade multiple such structures to obtain a broadband near-total absorber (Fig. 5). In particular, here we consider a structure with four unit cells, each consisting of two stubs. The geometrical parameters and imaginary part of the dielectric constant of the material filling each stub are chosen so that the absorption

resonance frequencies for the four structures are 173.4 THz, 184.4 THz, 193.4 THz, and 206.4 THz, respectively. The distance between two adjacent structures is 150 nm. Unlike the classical multilayer broadband absorbers, such as the so called Jaumann absorbers [7, 9], the distance between unit cells does not significantly impact the overall absorption performance in the forward direction due to the broadband near-zero reflection property. In Fig. 5(a) we observe that the near-total absorption wavelength range broadens as the number of cascaded unit cells increases. The absorption in the forward direction is more than 98% in a wide range of frequencies (168.4 THz to 208.4 THz) for the four unit cell case [Fig. 5(a)]. This is due to the fact that the overall absorption spectra are essentially the superposition of the absorption spectra of the individual perfect absorber unit cells, because of their broadband near-zero reflection property. In Fig. 5(b) we also show the magnetic field distributions at four different frequencies (173.4, 184.4, 193.4, and 206.4 THz). It is interesting to note that the absorbed power distribution in the structure is different at different frequencies. For example, when light is incident on the absorber at $f = 173.4$ THz and $f = 206.4$ THz, light is almost completely absorbed by the first and fourth cells, respectively [Fig. 5(b)]. This is similar to rainbow light trapping in slow light systems, where light waves are trapped at different positions at different frequencies [5, 49]. We also calculate the absorption spectra for a four unit cell structure where the same material properties are used in all unit cells ($\epsilon_A = 4.0804 - j0.68$, $\epsilon_B = 11.38 + j0.4$) [shown with blue circles in Fig. 5(a)], which are obtained by averaging the properties (ϵ_A and ϵ_B) of the four unit cells we used before. We observe that the absorption spectra of these two structures are almost identical. This relaxes the practical experimental requirements for our design, since the same gain and loss can be used in all unit cells. This is in fact possible because of the small geometrical differences among different unit cells. Note that the imaginary part of the dielectric constant of the gain material used in the broadband near-perfect absorber with four unit cells is 0.4, which corresponds to a gain coefficient of $g \approx 4800 \text{ cm}^{-1}$ [47]. The realization of gain coefficients of $\sim 5000 \text{ cm}^{-1}$ with optical pumping is within the limits of currently available semiconductor gain media [50]. In addition to the active material considered in this paper, a variety of other III-V semiconductor based optical gain media can be used. These include InGaAs [51], InGaAsP quantum well structures [52, 53], and InAs/GaAs quantum dot structures [54]. The use of quantum dot structures could lead to gain coefficients of more than 10^4 cm^{-1} [51, 54]. We also emphasize that the wavelength range of near-total absorption can be further widened by increasing the number of unit cells in the structure.

4. Conclusions

In this paper, we designed a non- PT -symmetric perfect absorber unit cell structure, consisting of two resonators side coupled to a waveguide, based on unidirectional reflectionlessness at exceptional points. Specifically, we considered a plasmonic waveguide-cavity system, consisting of two MDM stub resonators side coupled to a MDM waveguide. We used coupled mode theory to account for the behavior of the system. To obtain unidirectional total absorption, we used the coupled mode theory model, and optimized the geometric parameters of the structure, to eliminate the reflection and transmission in the forward direction at the optical communication wavelength. Using this approach, we found that the perfect absorber unit cell structure on resonance is a perfect reflector from one side and a perfect absorber from the other side. These findings were also confirmed by full-wave FDFD simulations.

Periodic PT -symmetric optical systems can support all-frequency unidirectional reflectionlessness at exceptional points by modulation of the complex refractive index profile. Here, we investigated the condition for broadband near-zero reflection in the forward direction of our proposed non- PT -symmetric perfect absorber unit cell system. We found that with proper design light can propagate through the absorber unit cell with near-zero reflection over a wide wavelength range. In addition, the proposed perfect absorber unit

cell is compact and suitable for ultradense chip-scale integration. Finally, we showed that, by cascading multiple properly designed unit cells, we obtain a structure in which light of different wavelengths can be almost completely absorbed at different positions in the structure. For such a structure the overall absorption spectra are essentially the superposition of the absorption spectra of the individual perfect absorber unit cells, and thus broadband near-total light absorption can be realized.

Our results could be potentially important for developing a new generation of highly compact unidirectional integrated nanophotonics devices. We also note that our proposal is scalable. In addition, the general design principle in our structures can be extended to other multiple layer systems, such as microwave structures with unidirectional invisibility.

As final remarks, we note that our proposed MDM waveguide based absorber is more compact and exhibits near-total absorption in a wider wavelength range compared to other MDM absorbers based on optical Tamm states [14]. In addition, the size of our proposed absorber could be further reduced by decreasing the guide wavelength through decreasing the width of the MDM waveguide [37]. We also found that, based on coupled mode theory, decreasing the decay rate of the field in the resonators due to the power escape through the waveguide (by separating the resonators and the waveguide with a small distance instead of directly coupling them [35]) could further increase the bandwidth of unidirectional reflectionlessness of the proposed perfect absorber unit cell. In addition, we note that the proposed broadband near-total absorbers can be realized in similar plasmonic waveguide-cavity systems based on other plasmonic two-conductor waveguides, such as three-dimensional plasmonic coaxial waveguides [55]. The proposed broadband near-total absorbers can also be realized by other structures such as microring and photonic crystal cavities [56, 57]. In such lossless structures gain media are not required to implement the proposed waveguide-cavity systems, since there is no internal loss in the resonators.

Funding

Postdoctoral Research Foundation of CSU; Foundation of the Key Laboratory of Optoelectronic Devices and Systems of Ministry of Education and Guangdong Province (GD201601); National Science Foundation (NSF) (1102301, 1254934); National Natural Science Foundation of China (NSFC) (61605252, 61422506).